

# DAViD: Modeling Dynamic Affordance of 3D Objects using Pre-trained Video Diffusion Models

Hyeonwoo Kim Sangwon Beak Hanbyul Joo  
Seoul National University

<https://snuvclab.github.io/david/>

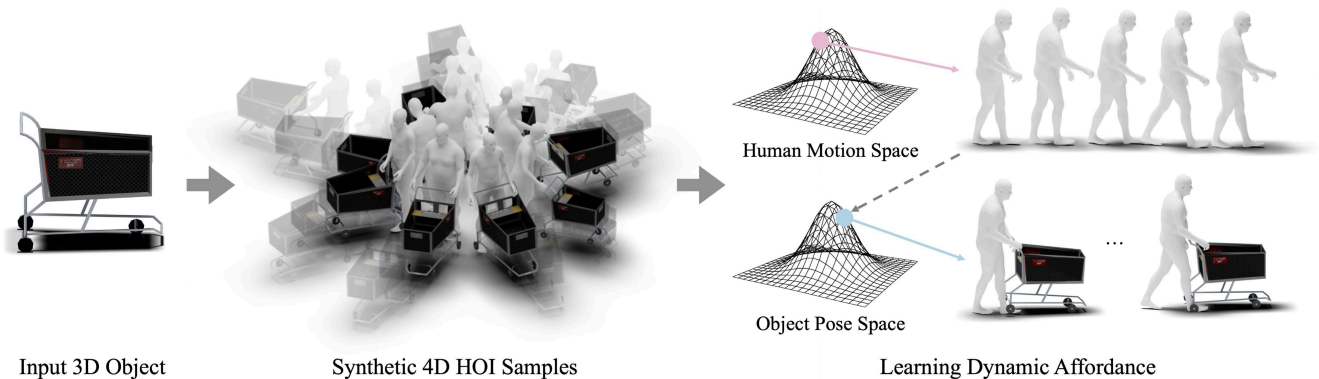


Figure 1. **Dynamic Affordance.** Given an input 3D object (left), our method learns Dynamic Affordance to model the dynamic patterns that occur during HOI (right). To build it, we present a framework to synthesize diverse 4D HOI samples (middle) by leveraging a pre-trained video diffusion model.

## Abstract

Understanding the ability of humans to use objects is crucial for AI to improve daily life. Existing studies for learning such ability focus on human-object patterns (e.g., contact, spatial relation, orientation) in static situations, and learning Human-Object Interaction (HOI) patterns over time (i.e., movement of human and object) is relatively less explored. In this paper, we introduce a novel type of affordance named *Dynamic Affordance*. For a given input 3D object mesh, we learn dynamic affordance which models the distribution of both (1) human motion and (2) human-guided object pose during interactions. As a core idea, we present a method to learn the 3D dynamic affordance from synthetically generated 2D videos, leveraging a pre-trained video diffusion model. Specifically, we propose a pipeline that first generates 2D HOI videos from the 3D object and then lifts them into 3D to generate 4D HOI samples. Once we generate diverse 4D HOI samples on various target objects, we train our DAViD, where we present a method based on the Low-Rank Adaptation (LoRA) module for pre-trained human motion diffusion model (MDM) and an object pose diffusion model with hu-

man pose guidance. Our motion diffusion model is extended for multi-object interactions, demonstrating the advantage of our pipeline with LoRA for combining the concepts of object usage. Through extensive experiments, we demonstrate our DAViD outperforms the baselines in generating human motion with HOIs.

## 1. Introduction

Humans effortlessly know how to appropriately utilize objects to achieve their goals in a given environment. This knowledge, also known as affordance [22], encapsulates a comprehensive understanding of how humans interact with specific objects. This affordance should consider not only the patterns such as contact, orientation, and position appearing in Human-Object Interaction (HOI) at a specific time instance but also the dynamic movements of humans and objects during interactions. For example, even when positioned directly behind the shopping cart, holding its handle and facing forward, we push the shopping cart ahead instead of lifting it up. Learning such affordances informs agents about how humans use objects and helps them act proactively

within their environments, making it crucial in the fields of robotics and AI. Given its importance, numerous studies on learning affordances [3, 11–14, 16, 38, 42, 52, 55, 57, 61–65, 71, 72, 75, 78, 79, 84, 92, 93, 97, 112, 120–122] appeared.

However, previous studies on affordance learning focus on patterns that occur in static HOIs. Some studies infer affordances in a given static context (typically provided as images) through contact on 2D images [4, 48], 3D humans [90, 109], and 3D objects [108, 109]. Others [27, 39] represent affordances as a distribution by aggregating patterns from various generated static HOI samples. While recent studies generate human motions including HOI [49, 50, 70, 104, 106, 107] and Human-Scene Interaction (HSI) [100, 104, 111], they focus on limited human motions (*e.g.*, stand and sit or pick and place) regardless of the object categories, which lack in capturing dynamic patterns appearing during real-world HOIs, which differ significantly depending on the object category.

In this paper, we introduce Dynamic Affordance, a novel type of affordance that models dynamic patterns in HOIs. The motivation for this concept arises from the observation that there are not only static patterns but also tendencies in the movements of both humans and objects over time during HOI. For instance, as shown in Fig. 2, we typically push a shopping cart and pull a suitcase while walking forward. We rarely lift the handles of the shopping cart and suitcase vertically. However, traditional studies based on static affordance (*e.g.*, relative position, contact) do not fully capture how humans interact with objects over time. We address this by training our DAViD which models the distribution of dynamic movements for both a human and an object during HOIs. Importantly, as we focus on modeling HOI motion depending on the object category, we treat human motion interacting with a specific object as a single concept and generate human motion faithful to that concept. To achieve this, we extend the human motion space by attaching Low-Rank Adaptation (LoRA) to a pre-trained motion diffusion model (MDM). Then, by modeling the remaining object motion space conditioned by human motion using a score-based diffusion model, we finally construct our Dynamic Affordance.

To train our DAViD, we need a dynamic human-object pair dataset involving diverse interactions. While most existing 3D HOI datasets provide dynamic sequences, they only focus on specific object categories [35, 98, 115] (*i.e.*, chair, ball), captured by marker-based capture methods [19, 29, 86, 118] which are difficult to scale. Furthermore, most existing datasets are captured in lab-controlled environments [5, 34, 40], making it challenging to obtain HOI data for various object categories. Our key observation for this is that a pre-trained video generation model can represent dynamic patterns of object usage in the form



Figure 2. **Dynamic Patterns in HOI.** People show dynamic patterns during HOI. Pre-trained video diffusion model has the knowledge of the dynamic patterns.

of videos. As shown in Fig. 2, the pre-trained video generation models already know how to generate videos with plausible dynamic patterns (*e.g.*, pushing a shopping cart, pulling a suitcase). However, leveraging a pre-trained video generation model to learn Dynamic Affordance presents two challenges: (1) the generated video should include HOI with an object that is geometrically identical to the given 3D object, and (2) both human and object motions in the video should be uplifted into a common 3D space. To address these challenges, we propose a Canny Edge [8] guided HOI image generation combined with an uplifting pipeline based on 2D correspondences.

We validate the efficacy of our approach by learning Dynamic Affordance on 30 3D object meshes from diverse categories, gathered from multiple sources [2, 5, 10, 34, 39, 60, 105]. We compare our Dynamic Affordance against existing methods [49] on the FullBodyManipulation dataset [49], showing that our model using synthetic samples, outperforms competitors on generating human motion including HOI. Additionally, we verify the advantage of Dynamic Affordance on generating human motion with multi-object interaction by training diffusion models using Dynamic Affordance. We will release the results and our source code.

In summary, our main contributions are summarized as: (1) we introduce a new type of affordance named Dynamic Affordance, which captures the distribution of both human motion and human conditioned object pose during interactions; (2) we propose a pipeline to generate diverse 4D HOI samples from 3D object mesh without laborious capturing; (3) we present a method for modeling the dynamic movements of humans in HOI as a single concept using LoRA and highlight its advantages in generating HOI motions that interact with multiple objects.

## 2. Related Work

**Reasoning Visual Affordance.** Affordance is a concept defined by Gibson [22] as the set of possible interactions that an agent can perform within an environment. As the concept narrows to the primary agent (or humans) and the specific interaction target (or objects), the area of learning

affordance mainly focuses on HOI. Specifically, followed by the intuition that the visual geometry of an object is closely related to its functionality, many studies leverage visual cues to reason about object’s affordance. The studies are subdivided into various areas, including affordance classification [42, 57, 72, 79, 84, 92, 93], affordance detection [3, 12, 16, 61, 63–65, 78], and affordance segmentation [13, 38, 55, 75]. Such traditional studies on affordance infer affordance for the given context (mostly provided as images), as a form of action labels [7, 32, 46], and contact regions in 2D [4, 48] or 3D [90, 108]. Later studies model static HOI patterns (*e.g.*, contact) during interactions [15, 27, 39], going beyond the understanding of individual HOI situations. Recent studies synthesize human motion including HOI [50, 70, 100, 104, 106, 107, 111], showing potential to learn dynamic HOI patterns, but they focus on a text-driven approach, generating quite consistent human motions regardless of object categories (*e.g.*, dragging a chair, holding a backpack). In contrast, our method focuses on learning dynamic HOI patterns of objects, observable in real-world HOIs.

**Learning from Synthesized Data.** Generative models such as GANs [23] and diffusion models are used as a strategy to address the problem of insufficient real-world data in many fields. Starting from augmentation [31, 66, 89, 103], synthetic datasets are widely used in vision area including segmentation [59, 91, 117], classification [9, 56, 87], shape reconstruction [68], and neural rendering [28, 116]. While data synthesis is a powerful technique that can be applied in many fields, the important thing to consider when learning from generated data is how reliable the generated data is compared to real-world data. Recently, few studies in the HOI field [27, 39] leverage pre-trained 2D diffusion model to generate 2D HOI images, demonstrating the reliability of synthetic data to learn affordance knowledge. While following the approaches, we focus on learning dynamic patterns during HOI rather than learning static patterns.

**Learning Concepts in Diffusion Models.** Concept learning, also known as concept customization, is a strategy to extend the space of the pre-trained model to understand specific concepts (*e.g.*, subjects, styles). Some studies tune the embeddings [21, 95] corresponding to a given concept in a pre-trained diffusion model, while others [44, 76] tune both the model weights and embeddings together. Recently, LoRA [33], originally used in large language models (LLMs), shows impressive results in producing images well aligned to the given concept [77], leading to an increase of attempts [26, 80, 82] to use LoRA for concept learning. Such concepts can be provided in various forms, including images [24, 51, 53, 119], videos [26, 102], and audios [96]. However, concept learning in fields beyond images, video, and audio is relatively less explored. We apply LoRA to the human motion space of pre-trained MDM [88] to learn

the dynamic patterns displayed in HOI as a single concept, extending the original human motion space in terms of HOI.

### 3. Method

Our approach aims to learn the dynamic affordance of a target object from synthetically generated 2D videos via a video diffusion model [1]. In the first stage, we generate diverse 4D HOI samples given a 3D object mesh of the target (Sec. 3.1). Then, our method models the collected 4D HOI samples into our DAViD, which consists of (1) a motion diffusion model to synthesize feasible human motions related to the target object along with LoRA, and (2) an object pose diffusion model to synthesize dynamic object motions paired with the synthesized human motion (Sec 3.2). An overview of our method is shown in Fig. 3.

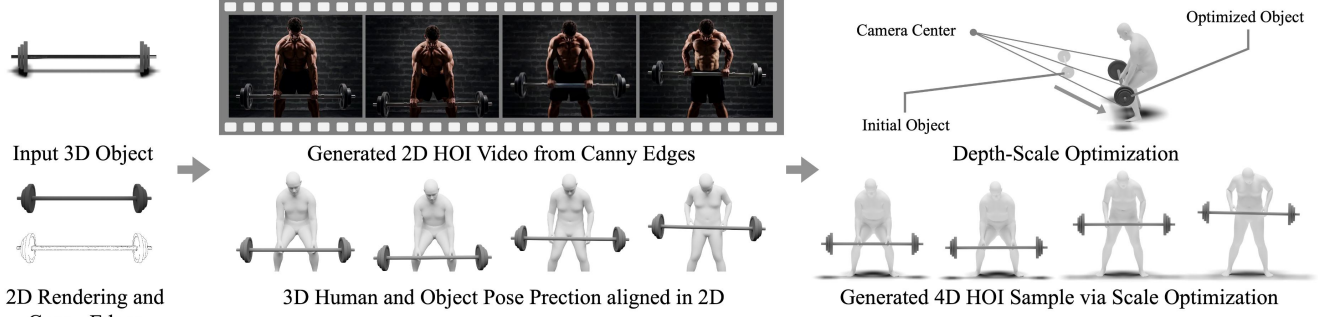
#### 3.1. 4D HOI Sample Generation

Our pipeline begins with a 3D mesh input for the target object and produces diverse 2D HOI videos showing how a person interacts with (or uses) the target object.

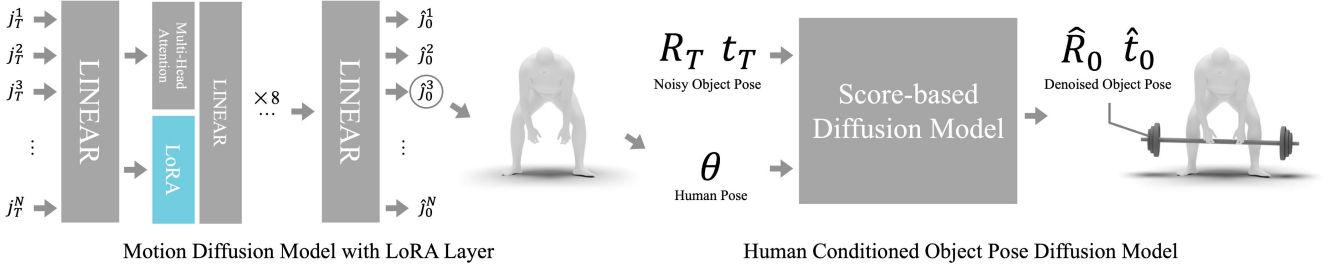
**2D HOI Video Synthesis.** Given an input 3D object mesh, we render it from multiple views using cameras  $\{\Pi_c\}_{c=1}^C$ . For the intrinsic parameters, we follow the perspective camera model of the world-grounded human mesh recovery method [81] which is used in our 3D lifting process, so that we can have a consistent camera setup. For the extrinsic parameters (camera viewpoints)  $\{\mathbf{R}_c, \mathbf{t}_c\}_{c=1}^C$ , we consider diverse commonly observable viewpoints for each object type (either ground-placed object or portable) with default object pose  $\{\mathbf{R}_o, \mathbf{t}_o\}$ , similar to the previous approach, ComA [39]. Specifically, for the relatively stationary ground-placed object (*e.g.*, motorcycle), we consider horizontal viewpoint variations centered on the target object, while for the portable objects (*e.g.*, trumpet), we render from the sampled viewpoint within a range. The object type is automatically inferred via a vision-language model [67], by querying with the rendered image with a query prompt, “Is the object plausible to be on the ground while it is being used?”.

After rendering the object, we synthesize a realistic human that naturally interacts with the rendered 2D object via an off-the-shelf pre-trained 2D diffusion model [45]. Unlike the previous approaches [39, 43, 110] for a similar goal that uses inpainting by providing a mask region where the inpainting model to fill, we synthesize the entire image via ControlNet [114], conditioning on the edge cues of rendered object [8]. Our primary motivation for this strategy is to synthesize not only plausible human-object interaction for the given object viewpoint but also the realistic background scene, which is important for 3D lifting, while preserving the pose and shape of the rendered object.

Once we synthesize HOI images for the target object from many views, we refine the generated 2D HOI images by manually filtering out low-quality or undesirable ones. As



(a) 4D HOI Sample Generation



(b) Learning Dynamic Affordance from Generated 4D HOI Samples

Figure 3. **Overview.** Our method consists of two parts: (1) Generating 4D HOI Samples and (2) Learning Dynamic Affordance from Generated 4D HOI Samples. First, we create 2D HOI videos, and generate 4D HOI samples with our uplifting pipeline. Then, the generated 4D HOI samples are used to train DAViD, learning the patterns of human motion and human pose conditioned object pose.

we only need a few-shot sample set to train our LoRA, this process requires minimal human effort, taking approximately three minutes per category.

Finally, we synthesize corresponding 2D HOI videos  $\{\mathcal{V}_d\}_{d=1}^N$  from the 2D HOI images  $\{\mathcal{I}_d\}_{d=1}^N$  by using a pre-trained image-to-video generation model [1] with the same text prompt used for generating images. It is noted that our synthesized 2D HOI videos have advantages over in-the-wild 2D real videos, which is crucial for 4D HOI sample generation: (1) our HOI videos contain diverse views and HOI scenarios for the known target 3D object, and (2) we know the corresponding camera parameters and the 3D object pose of the initial frame of the video.

**Uplifting for 4D HOI Sample Generations.** To uplift human motions into 3D from the synthesized 2D videos, we use an off-the-shelf world-grounded human motion recovery models, GVHMR [81] and TRAM [99], denoted as  $\mathbf{F}_{\text{human}}$ . We use GVHMR as the default method for module  $\mathbf{F}_{\text{human}}$  except in the scenarios where human translation occurs without walking motions (e.g., riding a motorcycle). In such cases, we use TRAM [99] instead, as GVHMR [81] typically fails to predict plausible camera motion under these conditions. Therefore,

$$\mathbf{F}_{\text{human}}(\mathcal{V}_d) = \{\theta_d^{f_i}, \beta_d^{f_i}, \mathbf{R}_d^{f_i}, \mathbf{t}_d^{f_i}, \mathbf{R}_{\text{cam},d}^{f_i}, \mathbf{t}_{\text{cam},d}^{f_i}\}_{i=1}^F, \quad (1)$$

where  $f_i$  is a superscript indicating that the term represents

the value at the  $i$ -th frame,  $\theta_d^{f_i} \in \mathbb{R}^{63 \times 3}$ ,  $\beta_d^{f_i} \in \mathbb{R}^{10}$ ,  $\mathbf{R}_d^{f_i} \in \text{SO}(3)$ ,  $\mathbf{t}_d^{f_i} \in \mathbb{R}^3$  are the predicted SMPL-X [69] human pose, shape, root joint’s rotation, and translation for  $i$ -th frame, respectively. The  $\mathbf{R}_{\text{cam},d}^{f_i} \in \text{SO}(3)$ ,  $\mathbf{t}_{\text{cam},d}^{f_i} \in \mathbb{R}^3$  are the rotation, and translation of estimated camera  $\Pi_d^{f_i}$ . Note that all of the parameters are defined in a world coordinate and we use default head and hand poses for the SMPL-X [69].

To obtain the remaining object motion, we first transform the default object pose with a transformation that transforms the camera used for object rendering to match the estimated camera  $\Pi_d^{f_1}$  in 3D space as follows:

$$\mathbf{R}_{o^\dagger}^{f_1} = \mathbf{R}_{\text{cam},d}^{f_1} (\mathbf{R}_{\gamma(d)})^{-1} \mathbf{R}_o \quad (2)$$

$$\mathbf{t}_{o^\dagger}^{f_1} = \mathbf{R}_{\text{cam},d}^{f_1} (\mathbf{R}_{\gamma(d)})^{-1} (\mathbf{t}_o - \mathbf{t}_{\gamma(d)}) + \mathbf{t}_{\text{cam},d}^{f_1}, \quad (3)$$

where  $\gamma(\cdot)$  is the function that maps the index of the 2D HOI image to the index of the camera from which it is rendered.  $\mathbf{R}_{o^\dagger}^{f_1}, \mathbf{t}_{o^\dagger}^{f_1}$  are each of the transformed object rotation and translation which is aligned with the first frame of the generated 2D HOI video. This is possible only for the first frame since the relative pose between camera and object used for object rendering corresponds only to the generated 2D HOI image, which is the first frame of the 2D HOI video. Our intuition for determining the object’s pose for later frames is to find the corresponding points of the object among 2D video frames, obtaining cues for the 3D pose of



the object. We first identify the 3D object vertices  $v_{o,3D} \in \mathbb{R}^{n_o \times 3}$  that are visible from the camera in the first frame  $\Pi_d^{f_1}$  by using raycasting [74]. For corresponding 2D rendered points  $v_{o,2D}^{f_1} = \Pi_d^{f_1}(v_{o,3D}) \in \mathbb{R}^{n_o \times 2}$  of the visible 3D object vertices  $v_{o,3D}$ , we utilize a 2D correspondence estimator [36, 37] to obtain the 2D corresponding points  $\{v_{o,2D}^{f_i}\}_{i=2}^F$  in the remaining video frames. As we have the 3D object vertices and the corresponding 2D matching points for each frame, we compute the camera poses for each frame with respect to the fixed object pose  $\{R_{o^\dagger}^{f_1}, t_{o^\dagger}^{f_1}\}$  using Perspective-n-Points (PnP) [20, 47] as follows:

$$\{R_{\text{rel}}^{f_i}, t_{\text{rel}}^{f_i}\} = \text{PnP}(v_{o,2D}^{f_i}, v_{o,3D}). \quad (4)$$

Using the estimated camera pose  $\Pi_d^{f_i}$  in world coordinate, we obtain the final object poses for each frame,  $\{R_{o^\dagger}^{f_i}, t_{o^\dagger}^{f_i}\}_{i=1}^F$  using the camera pose computed via PnP [20, 47] and applying a reverse transformation as follows.

$$R_{o^\dagger}^{f_i} = R_{\text{cam},d}^{f_i} \left( R_{\text{rel}}^{f_i} \right)^{-1} R_{o^\dagger}^{f_1} \quad (5)$$

$$t_{o^\dagger}^{f_i} = R_{\text{cam},d}^{f_i} \left( R_{\text{rel}}^{f_i} \right)^{-1} (t_{o^\dagger}^{f_1} - t_{\text{rel}}) + t_{\text{cam},d}^{f_i}. \quad (6)$$

**Resolving Scale-Depth Ambiguity.** Although we uplift human motion and object motion into a common 3D space, they are positioned along the rays so that their projections are matched to the 2D rendering, without considering their actual depth locations due to the scale-depth ambiguity. To resolve the ambiguity, we optimize the scale of the human ( $s_h$ ) and object ( $s_o$ ) in the camera direction using (1) a weak depth cue from the depth map, and (2) a contact cue from the object movement assumption. The loss term of weak depth cue is defined as follows:

$$\mathcal{L}_h = \left\| \left( s_h (v_{h,3D} - t_{h,d}^{f_1}) + t_{h,d}^{f_1} \right) - P_{h,3D} \right\|_2^2 \quad (7)$$

$$\mathcal{L}_o = \left\| \left( s_o (v_{o,3D} - t_{o,d}^{f_1}) + t_{o,d}^{f_1} \right) - P_{o,3D} \right\|_2^2, \quad (8)$$

where  $v_{h,2D} \in \mathbb{R}^{n_h \times 2}$ ,  $v_{h,3D} \in \mathbb{R}^{n_h \times 3}$  are visible 2D and 3D vertices of SMPL-X [69] in  $\mathcal{I}_d$  computed similarly as  $v_{o,2D}$ ,  $v_{o,3D}$ , and  $P_{h,3D}$ ,  $P_{o,3D}$  are 3D point cloud generated by projecting 2D metric depths (computed by metric depth model [6]) of  $v_{h,2D}$ ,  $v_{o,2D}$  into 3D space. Note that  $t_{h,d}^{f_1} \in \mathbb{R}^{n_h \times 3}$ ,  $t_{o,d}^{f_1} \in \mathbb{R}^{n_o \times 3}$  are expanded matrices of  $t_{\text{cam},d}^{f_1} \in \mathbb{R}^3$ , where each row of  $t_{h,d}^{f_1}$ ,  $t_{o,d}^{f_1}$  is the same as  $t_{\text{cam},d}^{f_1}$ . The loss term of the contact cue is defined as follows:

$$\mathcal{L}_{\text{HOI}} = d_n(P_H, P_O) \quad (9)$$

$$P_H = s_h (V_H - t_{H,d}^{f_1}) + t_{H,d}^{f_1} \quad (10)$$

$$P_O = s_o (V_O - t_{O,d}^{f_1}) + t_{O,d}^{f_1}, \quad (11)$$

where  $d_n(P_x, P_y)$  is the average distance of the  $n$  closest points of  $P_y$  to  $P_x$ , and  $V_O \in \mathbb{R}^{N_o \times 3}$ ,  $V_H \in \mathbb{R}^{N_h \times 3}$  are

point clouds consist of every vertex of object and human. Note that  $n$  is a hyperparameter that varies across categories, and  $t_{H,d}^{f_1} \in \mathbb{R}^{N_h \times 3}$ ,  $t_{O,d}^{f_1} \in \mathbb{R}^{N_o \times 3}$  are also expanded matrices of  $t_{\text{cam},d}^{f_1} \in \mathbb{R}^3$  where each row of  $t_{H,d}^{f_1}$ ,  $t_{O,d}^{f_1}$  is the same as  $t_{\text{cam},d}^{f_1}$ . Assuming that the object requires contact with the human to have movement, we set the loss to encourage the human and object to have contact points. We optimize the scale  $s_h$ ,  $s_o$  to obtain  $s_h^*$ ,  $s_o^*$  by minimizing total loss as follows:

$$\mathcal{L}_{\text{total}} = \mathcal{L}_h + \mathcal{L}_o + \mathcal{L}_{\text{HOI}} \quad (12)$$

As the original scale of human motion output by GVHMR [81] is already matched to real-world scale, we keep the scale of the human fixed and adjust the scale of the object by a factor of  $s_o^*/s_h^*$ . Since we use a perspective camera, the depth is also adjusted by the same ratio.

### 3.2. Learning Dynamic Affordance

Given the diverse dynamic 4D HOI samples we synthesized from a target 3D object, we pursue to build a generative motion model to learn the dynamic patterns of human and the target object. To learn such affordance, we propose DAViD, which consists of (1) LoRA [33] module to leverage a pre-trained MDM [88], and (2) human-conditioned object pose diffusion model. Our DAViD models both the distribution of human motion, and the distribution of object poses conditioned on human poses, enabling to generate diverse 4D HOI motion samples within the distributions.

**LoRA Module for MDM.** To learn the patterns of human motion interacting with a specific object, we insert a LoRA [33] layer into a pre-trained MDM [88] model and train the layer for each object. By choosing LoRA [33], we learn human motion patterns that are unseen in the pre-trained model, even with a small amount of training data. More interestingly, we find that by merging the trained LoRA [33] layers, it is possible to combine multiple human motion patterns during HOIs with a single model, which is previously unseen in the data samples.

In practice, we first consider the human motion part only without the object parts from 4D HOI samples previously generated, and preprocess the motion data following the method of HumanML3D [25], obtaining the training data of human joints denoted as  $\mathbf{j} \in \mathbb{R}^{F \times 22 \times 3}$ . Then, the LoRA [33] layer is added to the multi-head attention layer of the transformer encoder block in text-conditioned MDM [88] as shown in Fig. 3, and trained with the following joint recovery loss function.

$$\mathcal{L}(\Delta\phi) = \mathbb{E}_{j_0, t} \|j_0 - \mathcal{M}_{\phi + \Delta\phi}(j_t, t, c)\|_2^2, \quad (13)$$

where  $\phi$  is the original weight of pre-trained MDM [88] denoted as  $\mathcal{M}$ , and  $\Delta\phi$  is the weight of our LoRA [33] module we want to obtain. For the training text prompt, we use

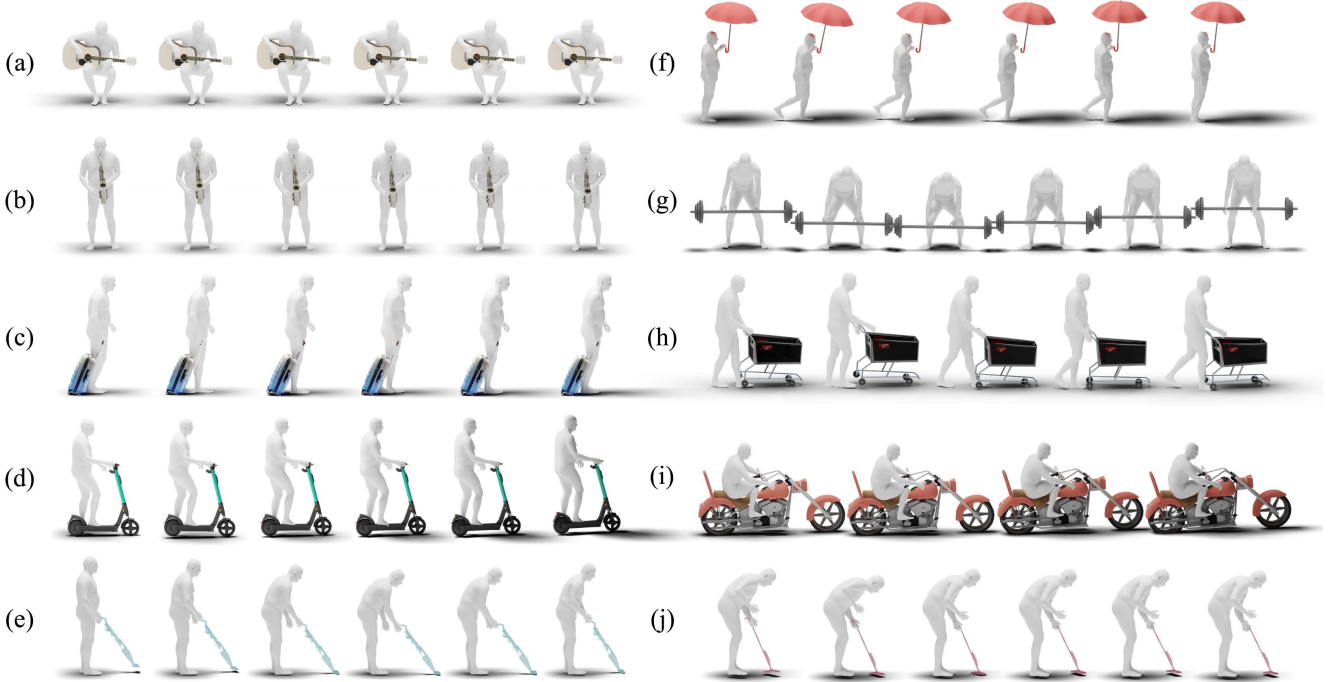


Figure 4. **Qualitative Results.** DAViD models the dynamic patterns of both a human and an object for various object categories. We visualize HOI motions for various objects generated by our DAViD, where frames are visualized in temporal order. The results show that our method effectively models the dynamic patterns emerging in HOIs.

automatically simplified text compared to the original used in 2D HOI image generation. See supplementary material for the detailed process.

**Human Conditioned Object Pose Diffusion.** Once we synthesize a plausible human motion, we then add a corresponding 3D object motion. As humans are the driving force behind an object’s movement, the motion of the object is inherently conditioned on the human’s motion. Specifically, we observe that the human pose at a specific timeframe is closely correlated to the object pose at the same time instance. Based on this intuition, we first (1) train a diffusion model that generates object poses conditioned on human poses, and then (2) provide smoothness guidance at inference time for the human motion condition, which we named Smoothness Guidance Sampling (SGS). In practice, we first sample 1024 vertices from the T-pose of SMPL-X [69] using Poisson disk sampling [58]. For the sampled indices, we normalize each frame of the generated 4D HOI sample by adjusting the translation so that the mean of the sampled human vertices aligns with the origin, and rotate the root orientation to align with z-axis of the world coordinate. Note that this transformation is applied to both the human and the object. A pair of the SMPL-X [69] body pose parameters  $\theta \in \mathbb{R}^{21 \times 3}$  and the normalized object pose  $\mathbf{p} \in \mathbb{R}^{3 \times 4}$  (consists of rotation and translation) is used for training our diffusion model. Using the dataset, our objective is to learn model  $\Psi$  which outputs the score function of conditional

object pose distribution for all noise level  $t$ .

$$\Psi(\mathbf{p}, t | \theta) = \nabla_{\mathbf{p}} \log p(\mathbf{p}_t | \theta) \quad (14)$$

According to Pascal et al. [94], the objective can be achieved by minimizing the following loss function.

$$\mathcal{L} = \mathbb{E}_{t \sim \mathcal{U}(\epsilon, 1)} \lambda(t) \mathbb{E}_{\mathbf{p}, t} \left\| \Psi_{\theta}(\mathbf{p}_t, t | \theta) - \frac{\mathbf{p}_0 - \mathbf{p}_t}{\sigma(t)^2} \right\|_2^2 \quad (15)$$

$$\sigma(t) = \sigma_{\min} \left( \frac{\sigma_{\max}}{\sigma_{\min}} \right)^t, \quad (16)$$

where  $\sigma_{\min} = 0.1$ ,  $\sigma_{\max} = 50$  are hyperparameters about noise perturbation. For the detailed structure of our score model, we follow the architecture of GenPose [113]. After training the conditional object pose diffusion model, we propose a simple but powerful technique to generate motion-like trajectories of the object at inference time called Smoothness Guidance Sampling (SGS). We estimate the object pose sequence  $\mathbf{p}^{f_1:f_F} \in \mathbb{R}^{F \times 3 \times 4}$ , which is conditioned on the body pose sequence  $\theta^{f_1:f_F} \in \mathbb{R}^{F \times 21 \times 3}$ . Instead of being guided solely on the estimated score from the model, we add a smoothness guidance term into the Probability Flow (PF) ODE [83] as follows:

$$\frac{d\mathbf{p}^{f_1:f_F}}{dt} = -\sigma(t)\dot{\sigma}(t)\Psi(\mathbf{p}^{f_1:f_F}, t, \theta^{f_1:f_F}) + \text{SGS}(\mathbf{p}_t^{f_1:f_F}), \quad (17)$$

where  $\text{SGS}(\mathbf{p}_i^{f_1:f_F})$  is the gradient of recovered  $\hat{\mathbf{p}}_0^{f_1:f_F} \in \mathbb{R}^{F \times 3 \times 4}$  from the given noise level of object pose on following smoothness loss.

$$\mathcal{L}_s(\hat{\mathbf{p}}_0^{f_1:f_F}) = \left\| \hat{\mathbf{p}}_0^{f_2:f_F} - \hat{\mathbf{p}}_0^{f_1:f_{F-1}} \right\|_2^2 \quad (18)$$

Note that we utilize RK45 ODE solver [17] for figuring out the ODE trajectory. SGS allows to find temporally smooth object pose trajectories while sampling each frame-wise pose in trained distribution.

## 4. Experiments

In this section, we conduct experiments to evaluate the efficacy of our method. In Section 4.3, we show various generated dynamic 3D HOI samples, demonstrating the efficacy of DAViD on learning dynamic patterns, and in Section 4.4, we conduct a quantitative comparison with other baselines. Finally, in Section 4.5, we introduce an application which shows the potential of our pipeline.

### 4.1. Datasets

For qualitative evaluation, we consider 30 input 3D object meshes from various sources, obtained from BEHAVE [5], InterCap [34], ShapeNet [10, 60], SAPIEN [105], FullBodyManipulation Dataset [49], and SketchFab [2]. For quantitative evaluation, we use FullBodyManipulation Dataset [49], which consists of the motion of both humans and objects. As our goal is to learn dynamic concepts of HOI using a few shots of 4D HOI samples, we conduct evaluations on object categories with relatively fewer long-tail interactions. Specifically, we use the mop object for the evaluation.

### 4.2. Baselines and Metric

Following previous approaches on generating human motion with HOI, we evaluate the quality of our generated 4D HOI samples against FullBodyManipulation Dataset [49] in terms of (1) human motion, and (2) interaction quality. Specifically, we use the state-of-the-art method of 4D HOI sample generation, OMOMO [49] as a baseline of comparison. However, while the baseline generates 4D HOI samples with object motion guidance, allowing for comparison with ground truth, our approach uses only a 3D object as input, making it challenging to define the ground truth of our generated samples. To address this, we evaluate the interaction quality of the generated samples via contact patterns, which is widely used in the area of affordance learning.

Specifically, we aggregate the contacts shown in each frame of the generated 4D HOI sample to compute contact scores for human joints. The contact score for each point is computed as a possibility of contact during the HOI. We use mean average error (MAE) [101] and similarity score (SIM) [85] to compare contact scores against FullBodyManipulation Dataset [49]. For the human joints, as we use

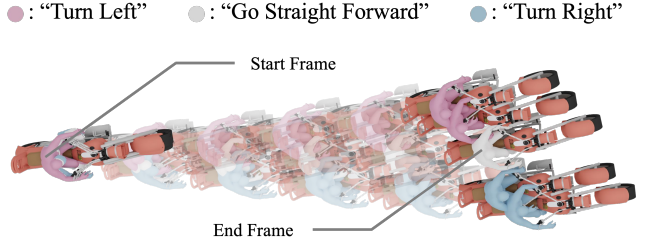


Figure 5. **Combining Concepts.** Human motion concept learned by our LoRA can be combined with original knowledge of pre-trained MDM.

the output format of SMPL-X [69] (with the default hand pose) instead of the baseline’s SMPL [54], we only consider the contact possibility of wrist joints which have structurally the same position. To remove the bias of the left and right hand, we add the possibility of contact of both wrist joints to construct the final contact score. Additionally, to assess human motion quality, we measure Foot Sliding (FS) [30] and foot height  $H_{\text{feet}}$  in centimeters (cm).

### 4.3. Qualitative Results

**4D HOI Generation for Various Objects.** Different from previous studies, we leverage the knowledge of a pre-trained video diffusion model, which allows to learn dynamic patterns of HOI for unbounded object categories objects. Fig. 4 visualizes the HOI motion for various objects generated by our DAViD. The frames are visualized in temporal order. The results show that our method effectively models the dynamic patterns naturally emerging in HOIs. In Fig. 4 (a) and Fig. 4 (b), we observe that the human pose and the relative position of the object are well modeled in relatively static HOI scenarios. In cases with more dynamic human motion, we find that various interaction patterns, including pulling—Fig. 4 (c), pushing—Fig. 4 (h), lifting—Fig. 4 (g), and holding—Fig. 4 (f) are well aligned with the typical use of objects of humans. Also, we can observe that our method can effectively capture complex human motions and their corresponding object motions, such as back and forth movement, as shown in Fig. 4 (e) and Fig. 4 (j). Importantly, unlike previous studies where motion translation typically resulted from walking, we observe that our model effectively captures cases of translation changes without foot movement, as shown in Fig. 4 (d) and Fig. 4 (h).

**Combining Multiple Concepts.** As we model dynamic patterns of human motion using LoRA [33] on a pre-trained MDM [88], the existing knowledge of MDM [88] can be combined with the newly learned concepts of human motion. Fig. 5 shows the result of combining the directional concept from the pre-trained MDM [88] with the motion of using a motorcycle, which we learned through LoRA [33]. Specifically, we use text prompts such as “A person turns

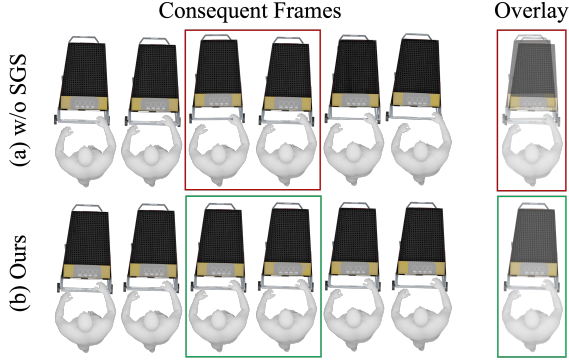


Figure 6. **Ablation on SGS.** SGS finds a smooth path that connects frame-wise plausible object poses at inference, increasing the plausibility of object motion.

Methods	$H_{feet} (\times 100) \downarrow$	FS $\downarrow$	$C_{SIM} \uparrow$	$C_{MAE} \downarrow$
Ours	<b>0.809</b>	<b>0.64</b>	<b>0.386</b>	<b>0.0654</b>
OMOMO [49]	1.52	2.68	0.273	0.113

Table 1. **Quantitative Results.** We evaluate the quality of generated HOI motion against FullBodyManipulation Dataset.

left riding a motorcycle”. Even without annotating direction knowledge during LoRA [33] tuning, we can combine our human motion concepts with the directional knowledge from the original MDM [88] to generate plausible HOI motion involving a motorcycle with change of direction.

**Ablation on Smoothness Guidance Sampling.** To verify the efficacy of our SGS, we conduct an ablation study. Fig. 6 shows six continuous frames of HOI motion with a shopping cart, along with an overlay of consequent two frames. Without SGS, object poses are independently computed for the human pose, causing motion jitters between adjacent frames and reducing the plausibility of the motion, as shown in Fig. 6 (a). In contrast, with our SGS, the generated HOI motion shows relatively smooth as shown in Fig. 6 (b). This shows the importance of SGS as it finds a path that continuously connects plausible object poses for each frame, creating a motion that is both frame-wise plausible and temporally smooth.

#### 4.4. Quantitative Results

To verify the efficacy of our trained DAViD, we compare OMOMO and ours on the FullBodyManipulation Dataset [49]. We compare the quality of HOI motion generated by OMOMO, trained on the FullBodyManipulation Dataset with ours generated from DAViD, which is trained using synthetic 4D HOI samples. Specifically, we generate 50 HOI motions per category using DAViD, while OMOMO [49] generates HOI motions in the same quantity as the test dataset in the FullBodyManipulation Dataset [49]. For evaluating human quality, we compute the FS and Foot

“A person rides a scooter while holding an umbrella”



Figure 7. **Generating Multi-Object Interaction.** Two human motion concepts learned by our LoRA is combined to generate multi-object interaction.

Height for each sample and then average them. As shown in Tab. 1, the quality of our human motion outperforms the baseline, indicating that our synthetic data is reliable enough to be comparable with real-world capture data. We demonstrate the effectiveness of our approach to learning from the synthetic data as it is easy to scale for various object categories. For evaluating interaction quality, we follow OMOMO [49] which focuses on comparing hand contact. We compute the hand contact score for both ours and baseline, and evaluate how similar these scores are to the hand contact score in the test set of FullBodyManipulation Dataset [49]. As shown in Tab. 1, the hand contact in our HOI motion accurately models the contact shown in the dataset than the baseline. According to the result, we demonstrate that our uplifting pipeline effectively decides spatial relations between humans and objects considering human-object contact, and consequently, DAViD well models the contact patterns.

#### 4.5. Application

As we learn human motion concepts using LoRA of the pre-trained MDM, it is possible to generate HOI motions with multi-object interactions by combining two different concepts. Specifically, we merge two separately trained LoRA parameters into the original network by a weighted summation, combining the two concepts into a single network. In practice, we assign the same weight value of 0.65 to each network parameter for summation. After merging the two LoRA models, we first generate human motion using the combined network, and then use this as a condition for the object pose diffusion model, obtaining each object’s pose sequence through SGS. Fig. 7 shows the result of combining two separately learned human motion concepts: one using a scooter and the other using an umbrella. We observe that the generated result shows plausible motion while satisfying the dynamic patterns of each object’s usage (*e.g.*, holding for the umbrella, riding for the scooter). By generating multi-object interactions through a simple plug-and-play approach with LoRA layers, we demonstrate the advantages of using LoRA to learn human motion concepts in HOI.



## 5. Discussion

In this paper, we present a method to learn an affordance called Dynamic Affordance and our framework DAViD which models it, addressing that there exists not only static patterns (*e.g.*, contact, spatial relation) but also dynamic patterns in HOIs. While obtaining a 4D HOI dataset including diverse objects is challenging, we observe that the video diffusion model has prior knowledge of the dynamic patterns for general objects. Compared to learning affordance from videos generated from text-to-video models, our pipeline, which first renders the 3D object to generate HOI images and then uses an image-to-video model, has the advantage of lifting affordances in video into 3D space. Using the 4D HOI samples generated through our lifting pipeline, we train DAViD, which consists of (1) the LoRA module of MDM for learning human motion patterns and (2) an object pose diffusion model with human pose guidance. We qualitatively show that the 4D HOI samples generated by DAViD effectively model the dynamic pattern of human pose and corresponding object pose during HOIs. Quantitative results show that our DAViD models human motion and interactions that are more similar to real-world HOI than the baseline. In addition, we demonstrate the advantage of using LoRA to model the dynamic patterns of using specific objects by generating HOI motion that include multi-object interactions.

## Acknowledgements

This work was supported by NAVER Webtoon, NRF grant funded by the Korean government (MSIT) (No. 2022R1A2C2092724, No. RS-2023-00218601), and IITP grant funded by the Korea government (MSIT) [No. RS-2024-00439854, RS-2021-II211343]. H. Joo is the corresponding author.

## References

- [1] Kling ai. <https://klingai.com/>, (accessed Nov 4th, 2024). 3, 4, 13
- [2] Sketchfab. <https://sketchfab.com/>, (accessed Oct 28th, 2024). 2, 7
- [3] Aitor Aldoma, Federico Tombari, and Markus Vincze. Supervised learning of hidden and non-hidden 0-order affordances and detection in real scenes. In *ICRA*, 2012. 2, 3
- [4] Shikhar Bahl, Russell Mendonca, Lili Chen, Unnat Jain, and Deepak Pathak. Affordances from human videos as a versatile representation for robotics. In *CVPR*, 2023. 2, 3
- [5] Bharat Lal Bhatnagar, Xianghui Xie, Ilya Petrov, Cristian Sminchisescu, Christian Theobalt, and Gerard Pons-Moll. Behave: Dataset and method for tracking human object interactions. In *CVPR*, 2022. 2, 7
- [6] Aleksei Bochkovskii, Amaël Delaunoy, Hugo Germain, Marcel Santos, Yichao Zhou, Stephan R. Richter, and Vladlen Koltun. Depth pro: Sharp monocular metric depth in less than a second. In *arXiv:2410.02073*, 2024. 5, 14
- [7] Minjie Cai, Kris M. Kitani, and Yoichi Sato. Understanding hand-object manipulation with grasp types and object attributes. In *RSS*, 2016. 3
- [8] John Canny. A computational approach to edge detection. In *IEEE TPAMI*, 1986. 2, 3, 13, 16
- [9] Lucy Chai, Jun-Yan Zhu, Eli Shechtman, Phillip Isola, and Richard Zhang. Ensembling with deep generative views. In *CVPR*, 2021. 3
- [10] Angel X. Chang, Thomas Funkhouser, Leonidas Guibas, Pat Hanrahan, Qixing Huang, Zimo Li, Silvio Savarese, Manolis Savva, Shuran Song, Hao Su, Jianxiong Xiao, Li Yi, and Fisher Yu. Shapenet: An information-rich 3d model repository. In *arXiv:1512.03012*, 2015. 2, 7
- [11] Yu-Wei Chao, Zhan Wang, Rada Mihalcea, and Jia Deng. Mining semantic affordances of visual object categories. In *CVPR*, 2015. 2
- [12] Chenyi Chen, Ari Seff, Alain Kornhauser, and Jianxiong Xiao. Deepdriving: Learning affordance for direct perception in autonomous driving. In *ICCV*, 2015. 3
- [13] Fu-Jen Chu, Ruinian Xu, and Patricio A. Vela. Learning affordance segmentation for real-world robotic manipulation via synthetic images. In *IEEE Robot. Autom. Lett.*, 2019. 3
- [14] Ching-Yao Chuang, Jiaman Li, Antonio Torralba, and Sanja Fidler. Learning to act properly: Predicting and explaining affordances from images. In *CVPR*, 2018. 2
- [15] Shengheng Deng, Xun Xu, Chaozheng Wu, Ke Chen, and Kui Jia. 3d affordancenet: A benchmark for visual object affordance understanding. In *CVPR*, 2021. 3
- [16] Thanh-Toan Do, Anh Nguyen, and Ian Reid. Affordancenet: An end-to-end deep learning approach for object affordance detection. In *ICRA*, 2018. 2, 3
- [17] J.R. Dormand and P.J. Prince. A family of embedded runge-kutta formulae. In *J. Comput. Appl. Math.*, 1980. 7
- [18] Patrick Esser, Sumith Kulal, Andreas Blattmann, Rahim Entezari, Jonas Müller, Harry Saini, Yam Levi, Dominik Lorenz, Axel Sauer, Frederic Boesel, Dustin Podell, Tim Dockhorn, Zion English, Kyle Lacey, Alex Goodwin, Yannik Marek, and Robin Rombach. Scaling rectified flow transformers for high-resolution image synthesis. In *arXiv:2403.03206*, 2024. 13
- [19] Zicong Fan, Omid Taheri, Dimitrios Tzionas, Muhammed Kocabas, Manuel Kaufmann, Michael J. Black, and Otmar Hilliges. Arctic: A dataset for dexterous bimanual hand-object manipulation. In *CVPR*, 2023. 2
- [20] Martin A Fischler and Robert C Bolles. Random sample consensus: a paradigm for model fitting with applications to image analysis and automated cartography. In *Commun. ACM*, 1981. 5, 13
- [21] Rinon Gal, Yuval Alaluf, Yuval Atzmon, Or Patashnik, Amit H. Bermano, Gal Chechik, and Daniel Cohen-Or. An image is worth one word: Personalizing text-to-image generation using textual inversion. In *ICLR*, 2023. 3
- [22] James J. Gibson. The ecological approach to visual perception. In *Houghton Mifflin*, 1979. 1, 2

- [23] Ian Goodfellow, Jean Pouget-Abadie, Mehdi Mirza, Bing Xu, David Warde-Farley, Sherjil Ozair, Aaron Courville, and Yoshua Bengio. Generative adversarial nets. In *NeurIPS*, 2014. 3
- [24] Yuchao Gu, Xintao Wang, Jay Zhangjie Wu, Yujun Shi, Chen Yunpeng, Zihan Fan, Wuyou Xiao, Rui Zhao, Shuning Chang, Weijia Wu, Yixiao Ge, Shan Ying, and Mike Zheng Shou. Mix-of-show: Decentralized low-rank adaptation for multi-concept customization of diffusion models. In *NeurIPS*, 2023. 3
- [25] Chuan Guo, Shihao Zou, Xinxin Zuo, Sen Wang, Wei Ji, Xingyu Li, and Li Cheng. Generating diverse and natural 3d human motions from text. In *CVPR*, 2022. 5, 15
- [26] Yuwei Guo, Ceyuan Yang, Anyi Rao, Zhengyang Liang, Yaohui Wang, Yu Qiao, Maneesh Agrawala, Dahua Lin, and Bo Dai. Animatediff: Animate your personalized text-to-image diffusion models without specific tuning. In *ICLR*, 2024. 3
- [27] Sookwan Han and Hanbyul Joo. Learning canonicalized 3d human-object spatial relations from unbounded synthesized images. In *ICCV*, 2023. 2, 3
- [28] Zekun Hao, Arun Mallya, Serge Belongie, and Ming-Yu Liu. Gancraft: Unsupervised 3d neural rendering of minecraft worlds. In *ICCV*, 2021. 3
- [29] Mohamed Hassan, Vasileios Choutas, Dimitrios Tzionas, and Michael J Black. Resolving 3d human pose ambiguities with 3d scene constraints. In *ICCV*, 2019. 2
- [30] Chengan He, Jun Saito, James Zachary, Holly Rushmeier, and Yi Zhou. Nemf: Neural motion fields for kinematic animation. In *NeurIPS*, 2022. 7
- [31] Ruifei He, Shuyang Sun, Xin Yu, Chuhui Xue, Wenqing Zhang, Philip Torr, Song Bai, and Xiaojuan Qi. Is synthetic data from generative models ready for image recognition? In *arXiv:2210.07574*, 2022. 3
- [32] Tucker Hermans, James M Rehg, and Aaron Bobick. Affordance prediction via learned object attributes. In *ICRA*, 2011. 3
- [33] Edward J Hu, Yelong Shen, Phillip Wallis, Zeyuan Allen-Zhu, Yuanzhi Li, Shean Wang, Lu Wang, and Weizhu Chen. Lora: Low-rank adaptation of large language models. In *ICLR*, 2022. 3, 5, 7, 8, 14, 15, 16, 17
- [34] Yinghao Huang, Omid Taheri, Michael J. Black, and Dimitrios Tzionas. Intercap: Joint markerless 3d tracking of humans and objects in interaction from multi-view rgb-d images. In *IJCV*, 2024. 2, 7
- [35] Nan Jiang, Tengyu Liu, Zhexuan Cao, Jieming Cui, Zhiyuan Zhang, Yixin Chen, He Wang, Yixin Zhu, and Siyuan Huang. Full-body articulated human-object interaction. In *ICCV*, 2023. 2
- [36] Nikita Karaev, Iurii Makarov, Jianyuan Wang, Natalia Neverova, Andrea Vedaldi, and Christian Rupprecht. Co-tracker3: Simpler and better point tracking by pseudo-labelling real videos. In *arXiv:2410.11831*, 2024. 5, 13
- [37] Nikita Karaev, Ignacio Rocco, Benjamin Graham, Natalia Neverova, Andrea Vedaldi, and Christian Rupprecht. Co-tracker: It is better to track together. In *ECCV*, 2024. 5, 13
- [38] David Inkyu Kim and Gaurav S. Sukhatme. Semantic labeling of 3d point clouds with object affordance for robot manipulation. In *ICRA*, 2014. 2, 3
- [39] Hyeonwoo Kim, Sookwan Han, Patrick Kwon, and Hanbyul Joo. Beyond the contact: Discovering comprehensive affordance for 3d objects from pre-trained 2d diffusion models. In *ECCV*, 2024. 2, 3, 13
- [40] Jeonghwan Kim, Jisoo Kim, Jeonghyeon Na, and Hanbyul Joo. Parahome: Parameterizing everyday home activities towards 3d generative modeling of human-object interactions. In *arXiv:2401.10232*, 2024. 2
- [41] Diederik P Kingma and Jimmy Ba. Adam: A method for stochastic optimization. In *arXiv:1412.6980*, 2014. 15, 16
- [42] Hedvig Kjellström, Javier Romero, and Danica Kragić. Visual object-action recognition: Inferring object affordances from human demonstration. In *CVIU*, 2011. 2, 3
- [43] Sumith Kulal, Tim Brooks, Alex Aiken, Jiajun Wu, Jimei Yang, Jingwan Lu, Alexei A. Efros, and Krishna Kumar Singh. Putting people in their place: Affordance-aware human insertion into scenes. In *CVPR*, 2023. 3
- [44] Nupur Kumari, Bingliang Zhang, Richard Zhang, Eli Shechtman, and Jun-Yan Zhu. Multi-concept customization of text-to-image diffusion. In *CVPR*, 2023. 3
- [45] Black Forest Labs. Flux. <https://blackforestlabs.ai/>, (accessed Nov 4th, 2024). 3, 13
- [46] Yong Jae Lee and Kristen Grauman. Predicting important objects for egocentric video summarization. In *IJCV*, 2015. 3
- [47] Vincent Lepetit, Francesc Moreno-Noguer, and Pascal Fua. Epnnp: An accurate o(n) solution to the pnp problem. In *IJCV*, 2009. 5, 13
- [48] Gen Li, Varun Jampani, Deqing Sun, and Laura Sevilla-Lara. Locate: Localize and transfer object parts for weakly supervised affordance grounding. In *CVPR*, 2023. 2, 3
- [49] Jiaman Li, Jiajun Wu, and C Karen Liu. Object motion guided human motion synthesis. In *ACM TOG*, 2023. 2, 7, 8
- [50] Jiaman Li, Alexander Clegg, Roozbeh Mottaghi, Jiajun Wu, Xavier Puig, and C. Karen Liu. Controllable human-object interaction synthesis. In *ECCV*, 2024. 2, 3
- [51] Zhen Li, Mingdeng Cao, Xintao Wang, Zhongang Qi, Ming-Ming Cheng, and Ying Shan. Photomaker: Customizing realistic human photos via stacked id embedding. In *CVPR*, 2024. 3
- [52] Wei Liang, Yibiao Zhao, Yixin Zhu, and Song-Chun Zhu. What is where: Inferring containment relations from videos. In *IJCAI*, 2016. 2
- [53] Zhiheng Liu, Ruili Feng, Kai Zhu, Yifei Zhang, Kecheng Zheng, Yu Liu, Deli Zhao, Jingren Zhou, and Yang Cao. Cones: Concept neurons in diffusion models for customized generation. In *arXiv:2303.05125*, 2023. 3
- [54] Matthew Loper, Naureen Mahmood, Javier Romero, Gerard Pons-Moll, and Michael J. Black. Smpl: A skinned multi-person linear model. In *Proc. ACM SIGGRAPH Asia*, 2015. 7
- [55] Timo Lüddecke and Florentin Wörgötter. Learning to segment affordances. In *ICCVW*, 2017. 2, 3

- [56] Chengzhi Mao, Augustine Cha, Amogh Gupta, Hao Wang, Junfeng Yang, and Carl Vondrick. Generative interventions for causal learning. In *CVPR*, 2021. 3
- [57] Tanis Mar, Vadim Tikhonoff, Giorgio Metta, and Lorenzo Natale. Self-supervised learning of tool affordances from 3d tool representation through parallel som mapping. In *ICRA*, 2017. 2, 3
- [58] Michael McCool and Eugene Fiume. Hierarchical poisson disk sampling distributions. In *Graphics Interface*, 1992. 6
- [59] Luke Melas-Kyriazi, Christian Rupprecht, Iro Laina, and Andrea Vedaldi. Finding an unsupervised image segmenter in each of your deep generative models. In *arXiv:2105.08127*, 2021. 3
- [60] Kaichun Mo, Shilin Zhu, Angel X. Chang, Li Yi, Subarna Tripathi, Leonidas J. Guibas, and Hao Su. Partnet: A large-scale benchmark for fine-grained and hierarchical part-level 3d object understanding. In *CVPR*, 2019. 2, 7
- [61] Bogdan Moldovan and Luc De Raedt. Occluded object search by relational affordances. In *ICRA*, 2014. 2, 3
- [62] Roozbeh Mottaghi, Connor Schenck, Dieter Fox, and Ali Farhadi. See the glass half full: Reasoning about liquid containers, their volume and content. In *ICCV*, 2017.
- [63] Austin Myers, Ching L. Teo, Cornelia Fermüller, and Yiannis Aloimonos. Affordance detection of tool parts from geometric features. In *ICRA*, 2015. 3
- [64] Anh Nguyen, Dimitrios Kanoulas, Darwin G. Caldwell, and Nikos G. Tsagarakis. Detecting object affordances with convolutional neural networks. In *IROS*, 2016.
- [65] Anh Nguyen, Dimitrios Kanoulas, Darwin G. Caldwell, and Nikos G. Tsagarakis. Object-based affordances detection with convolutional neural networks and dense conditional random fields. In *IROS*, 2017. 2, 3
- [66] Hyun-Jic Oh and Won-Ki Jeong. Diffmix: Diffusion model-based data synthesis for nuclei segmentation and classification in imbalanced pathology image datasets. In *arXiv:2306.14132*, 2023. 3
- [67] OpenAI. Gpt-4o system card. <https://openai.com/research/gpt-4v-system-card>, (accessed Nov 4th, 2024). 3, 13
- [68] Xingang Pan, Bo Dai, Ziwei Liu, Chen Change Loy, and Ping Luo. Do 2d gans know 3d shape? unsupervised 3d shape reconstruction from 2d image gans. In *arXiv:2011.00844*, 2020. 3
- [69] Georgios Pavlakos, Vasileios Choutas, Nima Ghorbani, Timo Bolkart, Ahmed A. A. Osman, Dimitrios Tzionas, and Michael J. Black. Expressive body capture: 3d hands, face, and body from a single image. In *CVPR*, 2019. 4, 5, 6, 7, 15, 16
- [70] Xiaogang Peng, Yiming Xie, Zizhao Wu, Varun Jampani, Deqing Sun, and Huaizu Jiang. Hoi-diff: Text-driven synthesis of 3d human-object interactions using diffusion models. In *arXiv:2312.06553*, 2023. 2, 3
- [71] Cody Phillips, Matthieu Lecce, and Kostas Daniilidis. Seeing glassware: from edge detection to pose estimation and shape recovery. In *RSS*, 2016. 2
- [72] Alessandro Pieropan, Carl Henrik Ek, and Hedvig Kjellström. Functional object descriptors for human activity modeling. In *ICRA*, 2013. 2, 3
- [73] Charles R. Qi, Li Yi, Hao Su, and Leonidas J. Guibas. Pointnet++: deep hierarchical feature learning on point sets in a metric space. In *NeurIPS*, 2017. 16
- [74] Scott D. Roth. Ray casting for modeling solids. In *Comput. Graph. Image Process.*, 1982. 5, 13, 14
- [75] Anirban Roy and Sinisa Todorovic. A multi-scale cnn for affordance segmentation in rgb images. In *ECCV*, 2016. 2, 3
- [76] Nataniel Ruiz, Yuanzhen Li, Varun Jampani, Yael Pritch, Michael Rubinstein, and Kfir Aberman. Dreambooth: Fine tuning text-to-image diffusion models for subject-driven generation. In *CVPR*, 2023. 3
- [77] Simo Ryu. Low-rank adaptation for fast text-to-image diffusion fine-tuning. (accessed Nov 15th, 2024). 3
- [78] Johann Sawatzky and Juergen Gall. Adaptive binarization for weakly supervised affordance segmentation. In *ICCVW*, 2017. 2, 3
- [79] Markus Schoeler and Florentin Wörgötter. Bootstrapping the semantics of tools: Affordance analysis of real world objects on a per-part basis. In *IEEE Trans. Cog. Develop. Sys.*, 2016. 2, 3
- [80] Viraj Shah, Nataniel Ruiz, Forrester Cole, Erika Lu, Svetlana Lazebnik, Yuanzhen Li, and Varun Jampani. Ziplora: Any subject in any style by effectively merging loras. In *ECCV*, 2024. 3
- [81] Zehong Shen, Huaijin Pi, Yan Xia, Zhi Cen, Sida Peng, Zechen Hu, Hujun Bao, Ruizhen Hu, and Xiaowei Zhou. World-grounded human motion recovery via gravity-view coordinates. In *Proc. ACM SIGGRAPH Asia*, 2024. 3, 4, 5, 13
- [82] Yujun Shi, Chuhui Xue, Jiachun Pan, Wenqing Zhang, Vincent YF Tan, and Song Bai. Dragdiffusion: Harnessing diffusion models for interactive point-based image editing. In *CVPR*, 2024. 3
- [83] Yang Song, Jascha Sohl-Dickstein, Diederik P Kingma, Abhishek Kumar, Stefano Ermon, and Ben Poole. Score-based generative modeling through stochastic differential equations. In *ICLR*, 2021. 6
- [84] Jie Sun, Joshua Moore, Aaron Bobick, and James Rehg. Learning visual object categories for robot affordance prediction. In *IJRR*, 2010. 2, 3
- [85] Michael J Swain and Dana H Ballard. Color indexing. In *IJCV*, 1991. 7
- [86] Omid Taheri, Nima Ghorbani, Michael J Black, and Dimitrios Tzionas. Grab: A dataset of whole-body human grasping of objects. In *ECCV*, 2020. 2
- [87] Fabio Henrique Kiyoyiti dos Santos Tanaka and Claus Aranha. Data augmentation using gans. In *arXiv:1904.09135*, 2019. 3
- [88] Guy Tevet, Sigal Raab, Brian Gordon, Yoni Shafir, Daniel Cohen-or, and Amit Haim Bermano. Human motion diffusion model. In *ICLR*, 2023. 3, 5, 7, 8, 15
- [89] Brandon Trabucco, Kyle Doherty, Max Gurinas, and Ruslan Salakhutdinov. Effective data augmentation with diffusion models. In *arXiv:2302.07944*, 2023. 3
- [90] Shashank Tripathi, Agniv Chatterjee, Jean-Claude Passy, Hongwei Yi, Dimitrios Tzionas, and Michael J. Black. Deco:

- Dense estimation of 3d human-scene contact in the wild. In *ICCV*, 2023. 2, 3
- [91] Nontawat Tritrong, Pitchaporn Rewatbowornwong, and Supasorn Suwajanakorn. Repurposing gans for one-shot semantic part segmentation. In *CVPR*, 2021. 3
- [92] Emre Ugur, Sandor Szedmak, and Justus Piater. Bootstrapping paired-object affordance learning with learned single-affordance features. In *ICDL*, 2014. 2, 3
- [93] Karthik Mahesh Varadarajan and Markus Vincze. Parallel deep learning with suggestive activation for object category recognition. In *ICVS*, 2013. 2, 3
- [94] Pascal Vincent. A connection between score matching and denoising autoencoders. In *Neural Comput.*, 2011. 6
- [95] Andrey Voynov, Qinghao Chu, Daniel Cohen-Or, and Kfir Aberman. P+: Extended textual conditioning in text-to-image generation. In *arXiv:2303.09522*, 2023. 3
- [96] Chenglong Wang, Jiangyan Yi, Xiaohui Zhang, Jianhua Tao, Le Xu, and Ruibo Fu. Low-rank adaptation method for wav2vec2-based fake audio detection. In *arXiv:2306.05617*, 2023. 3
- [97] Hanqing Wang, Wei Liang, and Lap-Fai Yu. Transferring objects: Joint inference of container and human pose. In *ICCV*, 2017. 2
- [98] Yinhuai Wang, Jing Lin, Ailing Zeng, Zhengyi Luo, Jian Zhang, and Lei Zhang. Physhoi: Physics-based imitation of dynamic human-object interaction. In *arXiv:2312.04393*, 2023. 2
- [99] Yufu Wang, Ziyun Wang, Lingjie Liu, and Kostas Daniilidis. Tram: Global trajectory and motion of 3d humans from in-the-wild videos. In *arXiv:2403.17346*, 2024. 4
- [100] Zan Wang, Yixin Chen, Baoxiong Jia, Puhao Li, Jinlu Zhang, Jingze Zhang, Tengyu Liu, Yixin Zhu, Wei Liang, and Siyuan Huang. Move as you say, interact as you can: Language-guided human motion generation with scene affordance. In *CVPR*, 2024. 2, 3
- [101] Cort J. Willmott and Kenji Matsuura. Advantages of the mean absolute error (mae) over the root mean square error (rmse) in assessing average model performance. In *Climate Research*, 2005. 7
- [102] Jianzong Wu, Xiangtai Li, Yanhong Zeng, Jiangning Zhang, Qianyu Zhou, Yining Li, Yunhai Tong, and Kai Chen. Motionbooth: Motion-aware customized text-to-video generation. In *NeurIPS*, 2024. 3
- [103] Weijia Wu, Yuzhong Zhao, Hao Chen, Yuchao Gu, Rui Zhao, Yefei He, Hong Zhou, Mike Zheng Shou, and Chunhua Shen. Datasetdm: Synthesizing data with perception annotations using diffusion models. In *NeurIPS*, 2023. 3
- [104] Zhen Wu, Jiaman Li, and C. Karen Liu. Human-object interaction from human-level instructions. In *arXiv:2406.17840*, 2024. 2, 3
- [105] Fanbo Xiang, Yuzhe Qin, Kaichun Mo, Yikuan Xia, Hao Zhu, Fangchen Liu, Minghua Liu, Hanxiao Jiang, Yifu Yuan, He Wang, Li Yi, Angel X. Chang, Leonidas J. Guibas, and Hao Su. Sapien: A simulated part-based interactive environment. In *CVPR*, 2020. 2, 7
- [106] Sirui Xu, Zhengyuan Li, Yu-Xiong Wang, and Liang-Yan Gui. Interdiff: Generating 3d human-object interactions with physics-informed diffusion. In *ICCV*, 2023. 2, 3
- [107] Sirui Xu, Ziyin Wang, Yu-Xiong Wang, and Liang-Yan Gui. Interdreamer: Zero-shot text to 3d dynamic human-object interaction. In *NeurIPS*, 2024. 2, 3
- [108] Yuhang Yang, Wei Zhai, Hongchen Luo, Yang Cao, Jiebo Luo, and Zheng-Jun Zha. Grounding 3d object affordance from 2d interactions in images. In *ICCV*, 2023. 2, 3
- [109] Yuhang Yang, Wei Zhai, Hongchen Luo, Yang Cao, and Zheng-Jun Zha. Lemon: Learning 3d human-object interaction relation from 2d images. In *CVPR*, 2024. 2
- [110] Yufei Ye, Xueting Li, Abhinav Gupta, Shalini De Mello, Stan Birchfield, Jiaming Song, Shubham Tulsiani, and Sifei Liu. Affordance diffusion: Synthesizing hand-object interactions. In *CVPR*, 2023. 3
- [111] Hongwei Yi, Justus Thies, Michael J. Black, Xue Bin Peng, and Davis Rempe. Generating human interaction motions in scenes with text control. In *ECCV*, 2024. 2, 3
- [112] Lap-Fai Yu, Noah Duncan, and Sai-Kit Yeung. Fill and transfer: A simple physics-based approach for containability reasoning. In *ICCV*, 2015. 2
- [113] Jiyao Zhang, Mingdong Wu, and Hao Dong. Generative category-level object pose estimation via diffusion models. In *NeurIPS*, 2023. 6, 15
- [114] Lvmin Zhang, Anyi Rao, and Maneesh Agrawala. Adding conditional control to text-to-image diffusion models. In *ICCV*, 2023. 3, 13
- [115] Xiaohan Zhang, Bharat Lal Bhatnagar, Sebastian Starke, Vladimir Guzov, and Gerard Pons-Moll. Couch: Towards controllable human-chair interactions. In *ECCV*, 2022. 2
- [116] Yuxuan Zhang, Wenzheng Chen, Huan Ling, Jun Gao, Yinnan Zhang, Antonio Torralba, and Sanja Fidler. Image gans meet differentiable rendering for inverse graphics and interpretable 3d neural rendering. In *ICLR*, 2021. 3
- [117] Yuxuan Zhang, Huan Ling, Jun Gao, Kangxue Yin, Jean-Francois Lafleche, Adela Barriuso, Antonio Torralba, and Sanja Fidler. Datasetgan: Efficient labeled data factory with minimal human effort. In *CVPR*, 2021. 3
- [118] Kaifeng Zhao, Shaofei Wang, Yan Zhang, Thabo Beeler, and Siyu Tang. Compositional human-scene interaction synthesis with semantic control. In *ECCV*, 2022. 2
- [119] Chenyang Zhu, Kai Li, Yue Ma, Chunming He, and Li Xiu. Multiboost: Towards generating all your concepts in an image from text. In *arXiv:2404.14239*, 2024. 3
- [120] Yuke Zhu, Alireza Fathi, and Li Fei-Fei. Reasoning about object affordances in a knowledge base representation. In *ECCV*, 2014. 2
- [121] Yuke Zhu, Ce Zhang, Christopher Ré, and Li Fei-Fei. Building a large-scale multimodal knowledge base system for answering visual queries. In *arXiv:1507.05670*, 2015.
- [122] Yixin Zhu, Chenfanfu Jiang, Yibiao Zhao, Demetri Terzopoulos, and Song-Chun Zhu. Inferring forces and learning human utilities from videos. In *CVPR*, 2016. 2



## A. Implementation Details

In this section, we introduce the details of our method for modeling Dynamic Affordance. From Sec. A.1 to Sec. A.4, we cover our first pipeline, 4D HOI Sample Generation. Sec. A.5 and Sec. A.6 describe our second pipeline, learning Dynamic Affordance.

### A.1. Rendering Object from Multi-Viewpoints

For camera installation, we position eight perspective cameras evenly spaced at  $45^\circ$  intervals around the object at a fixed elevation of  $5^\circ$ . The radius (distance of camera to origin) is set as a hyperparameter along with additional adjustment of camera’s z-coordinate to ensure the object fits within the image frame. To have a consistent camera setup in the uplifting pipeline, we follow GVHMR [81] and set the intrinsic parameters as follows.

$$K = \begin{bmatrix} f & 0 & w/2 \\ 0 & f & h/2 \\ 0 & 0 & 1 \end{bmatrix}, \quad (\text{S.19})$$

where  $f = \sqrt{h^2 + w^2}$  and  $h, w$  represent the height and width of our rendering image, respectively. In practice, we use  $h = 800, w = 1200$  for rendering. For object installation, relatively large and stationary ground-placed objects (e.g., motorcycles) are placed at the origin in a canonical state, while small and portable objects (e.g., umbrellas) are perturbed by sampling their position and rotation within a certain range. The range of the position and rotation is set as a hyperparameter.

### A.2. Generating 2D HOI images

For the image rendered in Sec. A.1, we use the Canny edge detector [8] to obtain structural guidance. In practice, we use an upper threshold of 30 and a lower threshold of 25 to capture dense structures. We use the obtained Canny edges as input of ControlNet [114] and leverage the off-the-shelf pre-trained 2D diffusion model, FLUX [45], to generate the 2D HOI Image. Unlike other approaches [39] that directly use inpainting on the rendered object, maintaining a consistent background color (e.g., white, gray), our method generate background, offering the advantage of aligning with the training domain of the video diffusion model while providing motion cues to the world-grounded HMR (e.g., if the background moves left, the subject moves right). For specific settings, we use a classifier-free guidance scale of 3.5, 28 inference steps, and the FlowMatchEulerDiscrete scheduler [18] for image generation. In cases where it is natural for a person to occlude an object (e.g., a hand occluding the handle of a cart), strong structural guidance can lead to the generation of implausible images. Therefore, we set the ControlNet [114] conditioning guidance as 0.725 for the first 12 denoising steps, and 0.0 for the later steps.

We empirically find that this approach helps generating plausible HOI image considering appropriate occlusion. For the text prompt for generating images, we use a vision-language model [67] to automatically obtain prompts that include HOI. Specifically, we obtain the text prompt using the following input.

*Write a text prompt in two sentence. The format of the text prompt should start with “1 person” and should include word “{category}”. Write a detailed text prompt focusing on human pose and the interaction between “1 person” and “{category}”. The third word of the first sentence must describe the interaction.*

We add the additional tag “, full body” at the end of the obtained text prompt, which we find beneficial for expressing the holistic body in image. While we know the category of the input 3D object in many cases, we use the rendering of the object to request a prompt if the category is not available.

### A.3. Generating 2D HOI Video from 2D HOI Image

We use a pre-trained video diffusion model [1] to generate 2D HOI videos from 2D HOI images. For the text prompt, we use the same one used for generating the 2D HOI image. As the video diffusion model support only specific resolution conditions, we resize both the input image and the output video.

### A.4. Lifting 2D HOI Videos to 4D HOI Samples

We detail the process of (1) computing object motion and (2) resolving depth ambiguity which are used to lift 2D HOI Videos into 4D HOI samples with additional figures (Fig. S.1, Fig. S.2).

**Obtaining Object Motion.** We leverage an off-the-shelf world-grounded HMR, GVHMR [81] to obtain both human motion and the corresponding camera motion in world coordinates. The core idea for obtaining the remaining object motion is to find 2D-3D correspondences for each frame. As we use a camera model same with GVHMR [81] for rendering, it is possible to transform (rotation and translation of) the rendering camera to the first frame camera of GVHMR’s output. Using the same transformation, we obtain the initial (first frame) object pose aligned with the human and camera motion. At the same time, we obtain the vertices of the object visible in the rendered camera through raycasting [74], and find the correspondences of 2D projection points across the generated 2D HOI Video via video tracking [36, 37]. Through this, we establish the 2D-3D correspondences of the vertices for each frame with known camera motion, allows PnP [20, 47] to compute object pose for each frame, as shown in Fig. S.1.

**Resolving Depth Ambiguity.** Even after obtaining the human motion, camera motion, and object motion aligned on

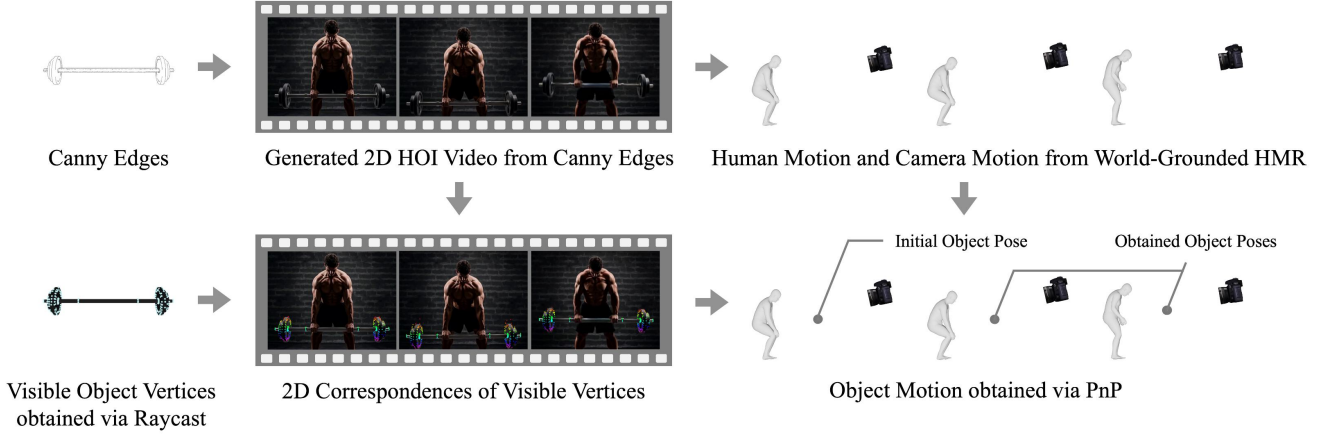


Figure S.1. **Obtaining Object Motion.** We first leverage off-the-shelf world-grounded HMR to obtain human motion and corresponding camera motion. Then, for the object vertices visible in our rendering camera, we find the 2D correspondences across the video. Using the 2D-3D correspondence of the vertices and camera pose for every frame, we compute the object pose for each frame via PnP.

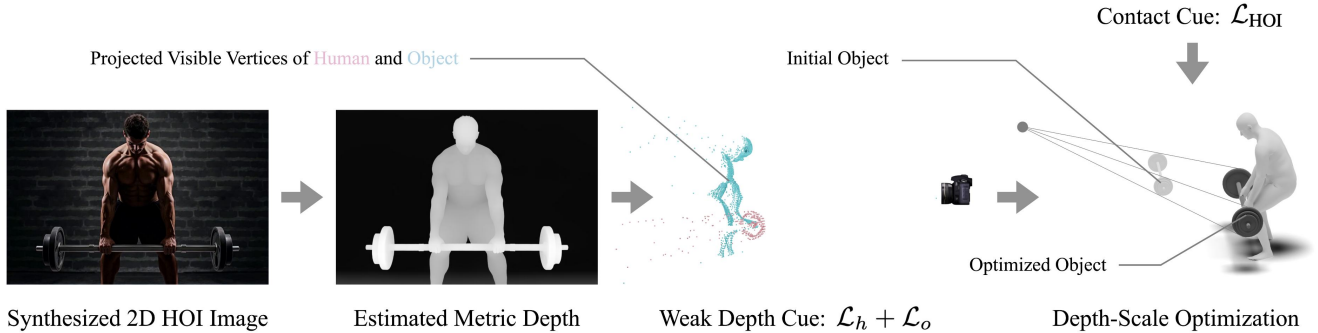


Figure S.2. **Resolving Depth Ambiguity.** To resolve the depth ambiguity between human and object motion, we leverage weak depth cues obtained from a metric depth model and contact cues, based on the intuition that object movement is driven by human contact. By optimizing the human and object scales using these cues, we obtain the 4D HOI sample.

2D, the human motion and object motion do not interact with each other in 3D space. To resolve the depth ambiguity that occurs on perspective camera rays, we optimize the object’s scale in the first frame using (1) weak depth cues and (2) contact cues. First, we use a publicly available depth estimation model [6] to predict the metric depth from the generated images. As shown in Fig. S.2, the visible vertices of the human and the object, obtained through raycasting [74] are projected into 3D space to construct a point cloud. The MSE distance between the human point cloud and the corresponding visible 3D vertices of the human is defined as  $\mathcal{L}_h$ , and we define  $\mathcal{L}_o$  similarly. Additionally, based on the intuition that the object must be in contact with the human to have movement, we define  $\mathcal{L}_{HOI}$  as the loss, calculated as the average distance of the  $n$  closest 3D vertices of the object to the 3D vertices of the human. In practice, we set  $n$  to one-third of the total number of vertices in the object mesh. We define the final loss as  $\mathcal{L}_{total} = \mathcal{L}_h + \mathcal{L}_o + \mathcal{L}_{HOI}$  and optimize the scales of the human and object,  $s_h$ , and  $s_o$ , to obtain to  $s_h^*$ ,

and  $s_o^*$ . To preserve the real-world scale of the human, we fix the human scale and only adjust the object’s scale by  $s_o^*/s_h^*$ .

### A.5. Network Architecture

We describe the network architecture of (1) LoRA for MDM and (2) the Human-Conditioned Object Pose Diffusion Model, which form our DAViD.

**LoRA for MDM.** To learn concepts through LoRA [33], we model the concepts represented by the samples using text prompts. To ensure that the text effectively models the concepts demonstrated by the given samples, we add LoRA [33] layers to the multi-head attention within the transformer encoder layer of the pre-trained MDM. Specifically, we add four 2-layer MLPs for query, key, value, and output projection, respectively for a single transformer encoder layer, allocating them as a space to learn additional knowledge. We add this to all 8 transformer encoder layers stacked in the transformer encoder.

**Human Conditioned Object Pose Diffusion Model.** To



(a) Generated HOI Motion for Other Categories



(b) Multiple Generated HOI Motion Samples

Figure S.3. **Additional Qualitative Results.** We showcase additional results of our method. As shown in (a), our method effectively models the patterns during HOI. Furthermore, in (b), we present diverse samples generated from our DAViD, with each frame visualized in temporal order.

model the conditional object pose based on the given human pose, we design a score-based diffusion model. We encode the object pose, timestep, and human pose using each MLP, concatenating the feature vectors to construct the total feature. The feature is then fed into three different MLPs, which output the scores for  $R_x$ ,  $R_y$ , and  $T$ , where  $R_x$  and  $R_y$  constitute the 6D rotation representation, and  $T$  represents the translation. The overall architecture is shown in Fig. S.4.

## A.6. Training Details

In this section, we describe the training details of (1) LoRA for MDM and (2) the Human Conditioned Object Pose Diffusion Model, which form our DAViD.

**LoRA for MDM.** For training the LoRA [33] layer in the pre-trained MDM [88], we create a dataset by extracting only the human motion from previously generated 4D HOI samples and processing it following HumanML3D [25]. The number of training samples varies by object category, ranging from 5 to 15, and we figure out that this amount is sufficient for learning the concept of human motion through

LoRA [33]. During training, we freeze all other weights and train only the weights of the LoRA [33] layer. As our concepts are represented in the form of text, we prepare training text prompt of (1) simplified text and (2) tag. The simplified text is a modified version of the text prompt used earlier for 2D HOI image generation (Sec. A.2), formatted as “A person {action} {category},” while the tag represents the category of an object. For each training sample, one of the two text prompts is assigned for training. We train a total of 500 to 3000 steps (depending on categories) using the Adam [41] optimizer with a learning rate of  $1 \times 10^{-4}$  without decay.

**Human Conditioned Object Pose Diffusion Model.** For training human conditioned object pose diffusion model, we extract pairwise human pose and object pose from each frame of the 4D HOI Sample and use them as training data. The number of data samples used varies by object category, ranging from 765 to 2,295. For human poses, we find that using the SMPL-X [69] body pose parameters  $\theta \in \mathbb{R}^{21 \times 3}$  produces qualitatively better results compared to using canonicalized point clouds used in GenPose [113]. To achieve

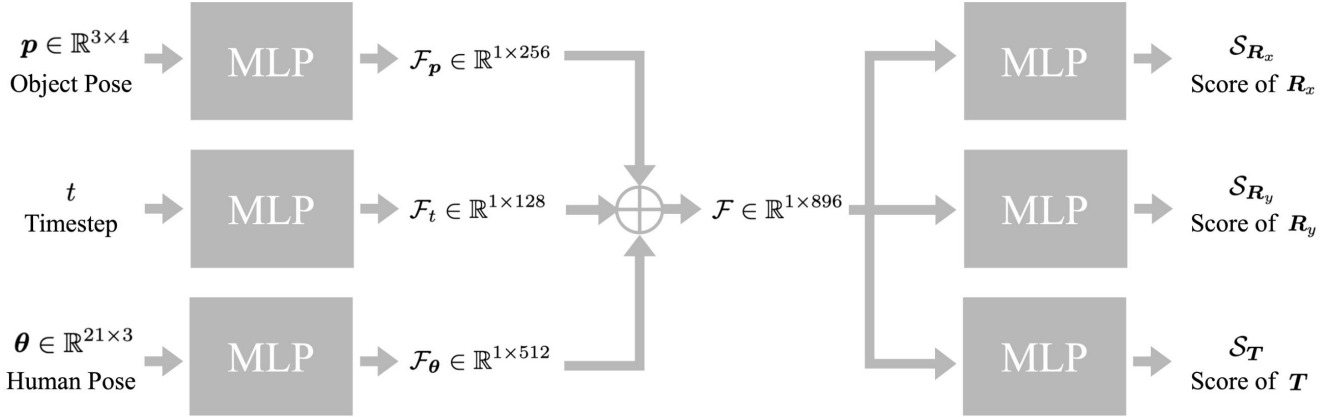


Figure S.4. **Architecture of Human Conditioned Object Pose Diffusion Model.** We design a diffusion model that generates a plausible object pose for interacting with a given human pose. Each object pose, time step, and human pose are encoded by MLP. The concatenated features then pass through different MLPs, producing an object pose output consisting of 6D rotation and translation.

this, we replaced the PointNet++ [73] encoder with 3-layer MLP. We train total of 1000 to 5000 steps (depending on categories) using the Adam [41] optimizer with a learning rate of  $5 \times 10^{-3}$  and a weight decay of 0.99.

## B. Experimental Details

### B.1. Additional Qualitative Results

We showcase additional qualitative results in Fig. S.3. In Fig. S.3(a), we show the results of training DAViD on additional object categories. As shown in the examples of the trumpet and cello, our method effectively models the relative position and orientation between human and the object, as well as the dynamic patterns, when playing instruments. Specifically, when using a trumpet, we observe a dynamic pattern where the hands hold the trumpet and keep it near the mouth while changing the head orientation. Similarly, when using a cello, we observe a dynamic pattern where the cello is positioned between the legs, and the right hand moves to play it. Fig. S.3(b) shows the results of generating various HOI motions using our trained LoRA [33]. Through the results of generating various HOI motions, we demonstrate that our LoRA [33] faithfully learns the dynamic patterns during HOI.

### B.2. Scale of the Object

As our human conditioned object pose diffusion model generates plausible object pose for a given human pose, it does not provide information about the object’s scale. Since the output human of MDM and the human in the training data both have a uniform scale of 1.0, we automatically determine the appropriate object scale in the generated HOI motion by sampling between the minimum and maximum scales of objects existing in our 4D HOI Samples.

## C. Limitations and Future Work

### C.1. Spatial Bias on 2D HOI Image Generation

Due to the internal spatial bias of the pre-trained 2D diffusion model, the model may fail to generate plausible images when structural guidance is introduced in locations that do not align with this bias, leading to collapse or hallucination. For example, if an umbrella, which should be held by a hand, is rendered at the bottom of the image and Canny edges [8] are extracted from it to generate an image, the model may create and use a new umbrella in a different location, rather than in the rendered region. As a future direction, we can consider a new form of conditional image generation that is guided only by the structure of the given object, without guidance on its location in the image. This approach is expected to remove the human labor we used for filtering malicious images.

### C.2. Limits of Smoothness Guidance Sampling

Although our human-conditioned object pose diffusion model is trained to generate plausible object pose during interactions given a human pose, our smoothness guidance sampling allows to generate plausible object motion for input sequential human poses. In many cases, the assumption that the object trajectory should be smooth while HOI is valid, but in situations where the object vibrates within a small range (e.g., when drilling a hole with an electric drill) colliding with other object, the assumption can be problematic. To naturally model motions involving such collisions, physics information is required, and understanding such physics during HOI can be considered as potential future work.

### C.3. Modeling Dexterous Hand-Object Interaction

Although we model the human with SMPL-X [69], and recent 2D diffusion models demonstrate impressive quality



in representing detailed hands, the pre-trained video diffusion model and 3D human estimator struggle to uplift the 2D hand from HOI images to high-quality 4D. This hinders the modeling of dexterous hand-object interactions in both our 4D HOI samples and the learned Dynamic Affordance. As a future direction, we can explore separately learning the hand patterns and merging them with the dynamic patterns we learned, with the expectation of improving the hand quality of the sampled HOI motion.

#### **C.4. Concept Conflict**

As we show that our LoRA [33] has an advantage for modeling multiple concepts (*e.g.*, combining existing knowledge of pre-trained model, and combining the knowledge of two individual LoRAs [33]), the concept conflict may appear when combining two different concepts, similar to what occurs in image diffusion models. When the two learned concepts show totally different human motion patterns (*e.g.*, lifting a barbell, pushing a cart), we empirically observe that the result converges into two cases: (1) a motion is interpolated between two concepts, resulting implausible motion or (2) one motion is performed followed by the other. Instead, when the two concepts are reasonably similar (*e.g.*, holding an umbrella, riding a scooter), their motions can be combined to generate multi-object interactions. However, we find that the relatively less coherent patterns (*e.g.*, the position of the hand while riding a scooter) are removed while combining the concepts, which is the limitation of our application.